Rare Metal Materials and Engineering
Volume 50, Issue 11, November 2021
Available online at www.rmme.ac.cn

Science Press

Cite this article as: Li Quan, Jin Zhaoyang. Comparative Study of Physical-Based Constitutive Model and BP Artificial Neural Network Model in Predicting High Temperature Flow Stress of AZ80 Magnesium Alloy[J]. Rare Metal Materials and Engineering, 2021, 50(11): 3924-3933.

ARTICLE

Comparative Study of Physical-Based Constitutive Model and BP Artificial Neural Network Model in Predicting High Temperature Flow Stress of AZ80 Magnesium Alloy

Li Quan, Jin Zhaoyang

School of Mechanical Engineering, Yangzhou University, Yangzhou 225127, China

Abstract: Based on the hot compression test data of as-cast AZ80 magnesium alloy under the conditions of deformation temperature of 250~400 °C and strain rate of 0.001~1 s^{-1}, a physical-based constitutive model based on the stress dislocation correlation and dynamic recrystallization dynamics and an artificial neural network (ANN) model based on feedforward backpropagation algorithm were established to predict the thermal deformation behavior of AZ80 magnesium alloy. Three statistical indicators, correlation coefficient (R), mean absolute relative error (AARE), and relative error (RE), were used to verify the prediction accuracy of these two models. The results show that both the models can accurately predict the thermal deformation behavior of AZ80 magnesium alloy. The stress value predicted by ANN model shows better agreement with the experimental data, and the value of R and AARE of ANN model is 0.9991 and 2.02%, respectively. While the R and AARE predicted by the physical-based constitutive model are 0.9936 and 4.52%, respectively. The better predictive ability of ANN model is attributed to its ability to deal with complex nonlinear relationships, while the predictive ability of the physical-based constitutive model is attributed to the fact that the model has certain physical meaning. The thermodynamic mechanism of work hardening (WH), dynamic recovery (DRV), and dynamic recrystallization (DRX) during thermal deformation are fully considered in the model parameters. Finally, the advantages and disadvantages of these two models are compared and discussed.

Key words: AZ80 magnesium alloy; physical-based constitutive model; artificial neural network model

Magnesium alloy is the lightest structural material which is widely used in modern industry due to its high strength, specific stiffness, good casting performance, good heat conduction, excellent electromagnetic shielding performance, and easy recycling. It is an ideal material for realizing lightweight component and resource reuse. According to the forming process, it can be divided into cast magnesium alloy and wrought magnesium alloy. The development of wrought magnesium alloy is an important part of magnesium alloy industry. Among all the wrought magnesium alloys, Mg-Al-Zn alloy is widely used due to its low price. AZ80 magnesium alloy is a high-strength alloy in the traditional Mg-Al-Zn series of wrought magnesium alloy, and has quite high ductility, good corrosion resistance, good oxidation resistance, and good welding performance, which can be manufactured into sheets, strips, profiles, bars, pipes, forgings, die forgings, and other mechanical parts under the medium load. In addition, the AZ80 alloy sheet can also be used as the skin, wall panel, and internal components of aircraft and missiles, and has broad application prospects in industry[1].

The room temperature deformation mechanism of AZ80 magnesium alloy is dominated by the basal slip and twinning which are easy to produce deformation texture, resulting in poor ductility of magnesium alloy and difficult plastic processing[2]. During high temperature deformation, AZ80 alloy with low stacking fault energy undergoes work hardening (WH) and dynamic softening, including dynamic recovery (DRV) and dynamic recrystallization (DRX), which makes the flow stress change with varying the deformation temperature, strain rate, and deformation degree. Therefore, the investigation of hot deformation laws of magnesium alloys is of great significance for the forming design and perfor-

Received date: November 07, 2020
Foundation item: National Natural Science Foundation of China (51901202); Natural Science Foundation of Jiangsu Province (BK20191442)
Corresponding author: Jin Zhaoyang, Ph. D., Professor, School of Mechanical Engineering, Yangzhou University, Yangzhou 225127, P. R. China, E-mail: zyjin@yzu.edu.cn

mance research of materials[3].

A constitutive model is the basis for describing the high-temperature flow characteristics of materials. It reveals the relationship between the flow stress and thermodynamic parameters of deformed materials, and can effectively reflect the dynamic response of materials during deformation. Generally, the flow behavior of materials under high temperature condition is the result of the combined effects of three thermodynamic mechanisms: WH, DRV, and DRX. Therefore, the establishment of an appropriate constitutive model is the prerequisite for accurately predicting the flow characteristics of materials. Lin et al[4] summarized the constitutive models established for metals or alloys in recent years, and classified them into three categories: phenomenological models[5,6], physical-based models[7-9], and artificial neural network (ANN) models[10-13].

Among the constitutive models, the phenomenological model is widely used to predict the high-temperature flow stress of materials due to its relatively simple calculation process without considering the physical mechanism in the process of thermal deformation. In order to further improve the prediction accuracy of the model, it is necessary to consider the physical meaning during the thermal deformation. Based on the classic stress-dislocation correlation and DRX kinetics, researchers established the two-stage constitutive models of firstly considering WH-DRV mechanism and then considering DRX mechanism for 42CrMo steel, 7050 aluminum alloy, and nickel-based alloy[7-9], which comprehensively contained the mechanism and thermal deformation behavior of DRV and DRX processes. These models have certain physical significance, and the results show that they have a good predictive ability. However, the application of the two-stage constitutive model in magnesium alloys is rarely reported.

The ANN model does not need to assume a mathematical model and determine its parameters in advance, which provides a new way to predict the deformation behavior of materials under different conditions. In general, the deformation response of materials at high temperature is highly nonlinear, and many factors affecting the flow characteristics of materials are also nonlinear-related, which reduces the accuracy of the regression method in predicting the flow stress. Neural network models are good at solving the difficult problems in traditional calculation methods, especially for the complex nonlinear relationships. Peng et al[10] established a backpropagation (BP) neural network model for as-cast Ti60 aluminum alloy with the mean absolute relative error (AARE) of 2.41%. Haghdadi et al[11] established a BP neural network model for A356 aluminum alloy, and its AARE between the experiment results and predicted values was 1.2%. Yan et al[12] established a BP neural network model for Mg-5.9Zn-1.6Zr-1.6Nd-0.9Y alloy with AARE of 2.853%. The results show that ANN model can predict the flow stress of different materials effectively and accurately.

Based on the experiment data of hot compression tests, the physical-based constitutive model and BP ANN model for AZ80 magnesium alloy were established in this research. The prediction accuracy of flow stress according to these two models was compared quantitatively, and the advantages, disadvantages, and applicability of these two models were discussed, laying a foundation for simulation and process optimization of thermal deformation process of as-cast AZ80 magnesium alloy.

1 Experiment

As-cast AZ80 magnesium alloy was used in this research, and its chemical composition is shown in Table 1. In order to reduce the residual stress and non-uniform deformation, the as-cast AZ80 magnesium alloy was homogenized before hot compression tests. The specimens were kept at 400 °C for 12 h to eliminate the second phase and dendritic structure. The hot compression specimen was a cylinder with the dimension of Φ8 mm×12 mm. The specimen surface was smooth. The hot compression tests were conducted on Gleeble-3500D thermal simulation test machine. The deformation temperature was 250, 300, 350, and 400 °C, and the strain rate was 0.001, 0.01, 0.1, and 1 s^{-1}. The maximum deformation of the specimen was 60%. The hot compressed specimens were heated to a specified temperature with a heating rate of 5 °C/s, and then kept at the temperature for 180 s to make sure that every part of the specimens was at the same temperature. After the hot compression test, the specimens were quenched immediately to retain the high temperature structure.

2 Results and Discussion

The true stress-strain curves of AZ80 magnesium alloy under thermal compression are shown in Fig.1. It can be seen that the deformation temperature and strain rate have significant effects on flow stress. At a specific strain rate, the flow stress is increased with decreasing the deformation temperature; at a specific temperature, the flow stress is increased with increasing the strain rate. This is because the thermal deformation of the material results from the combination of WH and dynamic softening.

According to the dynamic softening mechanism of the thermal deformation process, the flow stress-strain curve can be divided into two categories: DRV and DRX, as shown in Fig. 2. DRV is the main softening mechanism. At the beginning of deformation, due to the leading role of WH and DRV, the flow stress is increased rapidly until the peak stress σ_p. When the equilibrium between WH and DRV is reached, the saturation stress σ_{sat} occurs. However, for the DRX curve, as the amount of deformation increases, when the strain is greater than the critical strain, the material undergoes DRX process. Thereafter, WH, DRV, and DRX jointly affect the flow stress of the material. As the deformation continues, the

Table 1 Chemical composition of AZ80 magnesium alloy (wt%)

Al	Zn	Mn	Si	Fe	Ni	Cu	Mg
8.360	0.524	0.385	0.076	0.005	0.006	0.003	Bal.

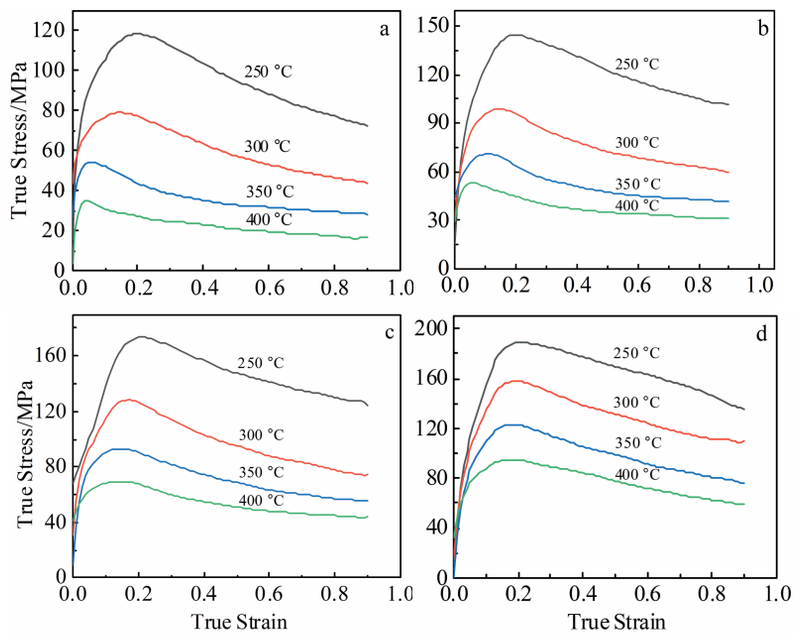

Fig.1 True stress-true strain curves of AZ80 magnesium alloys at different strain rates: (a) $\dot{\varepsilon}$=0.001 s^{-1}, (b) $\dot{\varepsilon}$=0.01 s^{-1}, (c) $\dot{\varepsilon}$=0.1 s^{-1}, and (d) $\dot{\varepsilon}$=1 s^{-1}

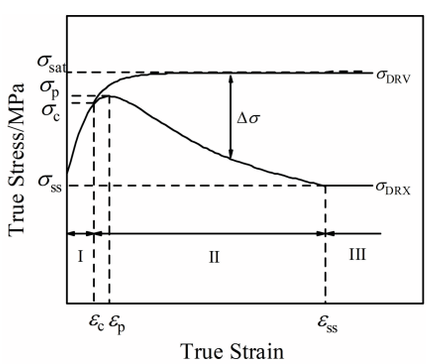

Fig.2 Typical stress-strain curves of AZ80 magnesium alloy

softening effect of DRX gradually becomes obvious, and the flow stress firstly increases to the peak stress σ_p, and then gradually decreases.

3 Establishment of Constitutive Models

3.1 Establishment of physical-based constitutive model

According to the characteristics of hot compression deformation behavior of AZ80 magnesium alloy, the constitutive models of two-stages of WH-DRV and DRX were established.

3.1.1 Constitutive model of WH-DRV stage

The evolution of dislocation density with strain is generally controlled by the competition between dislocation storage and dislocation disappearance. The relationship between dislocation density and strain can be expressed as follows[7]:

$$\frac{\mathrm{d}\rho}{\mathrm{d}\varepsilon} = U - \Omega\rho \tag{1}$$

where $\mathrm{d}\rho/\mathrm{d}\varepsilon$ is the increase rate of dislocation density with strain, ρ is the dislocation density, U stands for WH and can be regarded as a parameter of strain, Ω is the DRV coefficient, and $\Omega\rho$ is the DRV caused by dislocation disappearance and rearrangement[14]. The integration of Eq. (1) can be expressed as follows:

$$\rho = \frac{U}{\Omega} - \left(\frac{U}{\Omega} - \rho_0\right)\mathrm{e}^{-\Omega\varepsilon} \tag{2}$$

where ρ_0 is the initial dislocation density. The classic relationship of flow stress-dislocation density[15] is $\sigma=\alpha\mu b\sqrt{\rho}$, where α is the material parameter, μ is the shear modulus, and b is a Burgers vector mode. By substituting the expression into Eq. (2), the flow stress in WH-DRV stage can be expressed as follows:

$$\sigma = \left[\sigma_{\mathrm{sat}}^2 + \left(\sigma_0^2 - \sigma_{\mathrm{sat}}^2\right)\mathrm{e}^{-\Omega\varepsilon}\right]^{0.5} \tag{3}$$

where σ is the flow stress; the saturation stress σ_{sat} and the yield stress σ_0 are equal to $\alpha\mu b\sqrt{U/\Omega}$ and $\alpha\mu b\sqrt{\rho_0}$, respectively.

According to Eq. (3), it can be known that three parameters (σ_{sat}, σ_0, Ω) should be determined. The saturation flow stress σ_{sat} is usually determined by the relationship between WH rate $\theta=\mathrm{d}\sigma/\mathrm{d}\varepsilon$ and the flow stress σ, as shown in Fig. 3. Firstly, the inflection point of the θ-σ curve can be obtained (represented by the rectangular symbol in Fig. 3). Then, the saturated flow stress σ_{sat} is equal to the horizontal intercept of the tangent line of the θ-σ curve passing through the inflection point. When $-|\mathrm{d}\theta/\mathrm{d}\sigma|$ reaches the minimum value, it corresponds to the inflection point of the θ-σ curves, which is also the critical condition for DRX initiation[16]. The inflection points of the θ-σ curves and the peak points of the true stress-strain curves can reveal the occurrence of DRX. It can

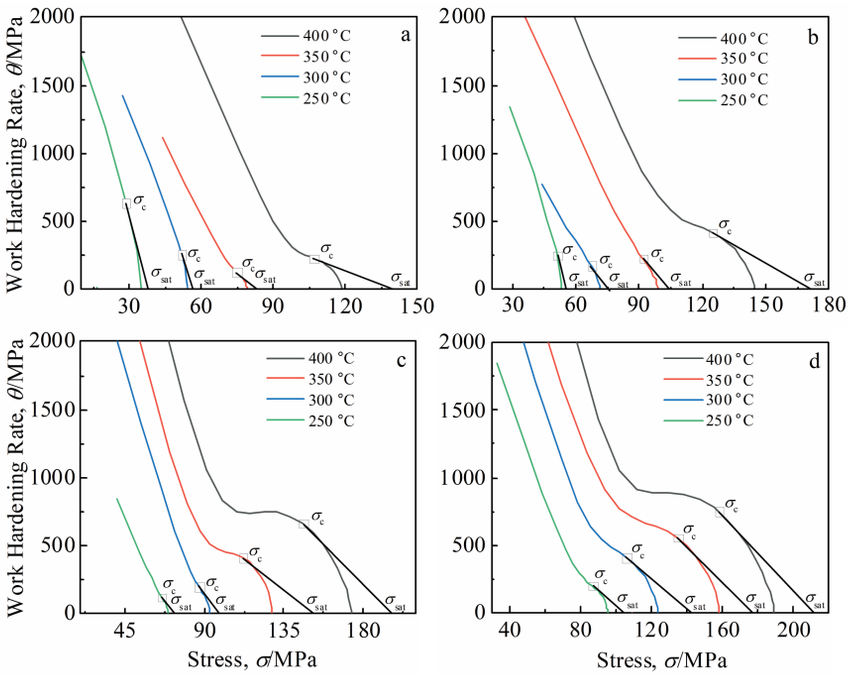

Fig.3 Relationships between WH rate θ and stress σ at different strain rates: (a) $\dot{\varepsilon}$=0.001 s^{-1}, (b) $\dot{\varepsilon}$=0.01 s^{-1}, (c) $\dot{\varepsilon}$=0.1 s^{-1}, and (d) $\dot{\varepsilon}$=1 s^{-1}

be seen from Fig.3a~3d that all curves have inflection points, which clearly shows that DRX occurs in the deformation process.

The results show that the saturated flow stress σ_{sat} can be expressed as a function of the peak stress σ_p by Eq. (4), as follows:

$$\sigma_{sat} = -23.88 + 1.44\sigma_p \quad (4)$$

Fig. 4 shows the experiment results and the fitting line obtained according to Eq.(4).

In general, the effects of deformation temperature and strain rate on flow stress can be characterized by Zener-Hollomon parameter, namely Z parameter[17], and the expression of Z parameter can be expressed as follows:

$$Z = \dot{\varepsilon}\exp\left(\frac{Q}{RT}\right) \quad (5)$$

where $\dot{\varepsilon}$ is the strain rate (s^{-1}), T is the absolute temperature (K), R is the ideal gas constant (8.314 $J\cdot mol^{-1}\cdot K^{-1}$), and Q is the deformation activation energy ($J\cdot mol^{-1}$). In order to obtain the value of Z parameter, the deformation activation energy Q should be calculated firstly, and the detailed calculation procedure was reported in Ref. [18]. The Q value of AZ80 alloy is estimated as 177 332 $J\cdot mol^{-1}$.

Based on the flow stress-strain curve, the yield stress σ_0 at different deformation temperatures and strain rates can be directly obtained. Fig. 5 shows the relationship between the yield stress σ_0 and the Z parameter. It is clear that there is a good linear relationship, so the yield stress σ_0 can be expressed as a function of the Z parameter, as follows:

$$\sigma_0 = 0.40\ln Z + 1.43 \quad (6)$$

According to Eq. (3), the DRV coefficient Ω can be calculated by Eq.(7), as follows:

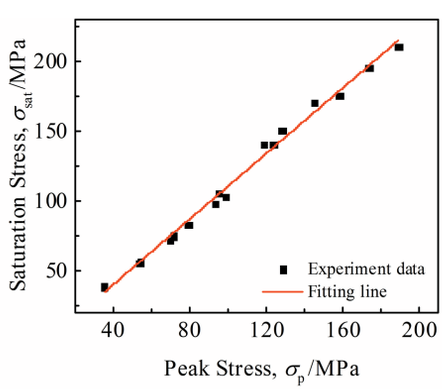

Fig.4 Relationship between saturation stress σ_{sat} and peak stress σ_p

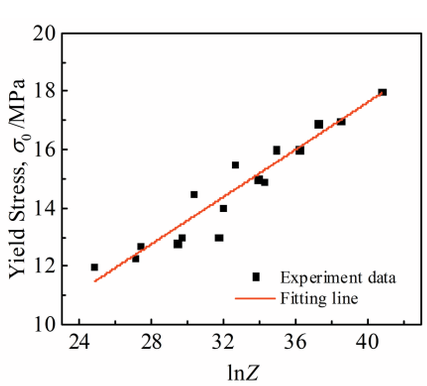

Fig.5 Relationship between yield stress σ_0 and ln$Z$

$$\Omega\varepsilon = \ln\left(\frac{\sigma_{sat}^2 - \sigma_0^2}{\sigma_{sat}^2 - \sigma^2}\right) \quad (7)$$

Based on the flow stress-strain curves before reaching the critical strain, the Ω values can be calculated. Fig.6 shows the relationship between Ω and Z parameter. It can be found that the DRV coefficient is increased with decreasing the Z parameter, and Ω can be expressed as an exponential function of the Z parameter, as follows:

$$\Omega = 68.8851Z^{0.06451} \quad (8)$$

Therefore, the constitutive equations for the as-cast AZ80 magnesium alloy during the WH-DRV stage can be expressed as follows:

$$\begin{cases} \sigma_{DRV} = \left[\sigma_{sat}^2 + \left(\sigma_0^2 - \sigma_{sat}^2\right)e^{-\Omega\varepsilon}\right]^{0.5} \\ \sigma_{sat} = -23.88 + 1.44\sigma_p \\ \sigma_0 = 0.40\ln Z + 1.43 \\ \Omega = 68.8851Z^{0.06451} \\ Z = \dot{\varepsilon}\exp(177\,332/RT) \end{cases} \quad (9)$$

3.1.2 Constitutive model of DRX stage

When the deformation degree is greater than the critical strain ε_c, the DRX grains nucleate and grow near the grain boundaries, twin boundaries, and deformation bands. At higher deformation temperature and lower strain rate, DRX occurs more obviously.

In this research, the classic Avrami equation was used to describe the DRX behavior of as-cast AZ80 magnesium alloy, i.e., the DRX volume fraction (X_{DRX}) can be expressed as the function of the strain ε[19], as follows:

$$X_{DRX} = 1 - \exp\left[-K_d\left(\frac{\varepsilon - \varepsilon_c}{\varepsilon_p}\right)^{n_d}\right] \quad (\varepsilon \geq \varepsilon_c) \quad (10)$$

where K_d and n_d are undetermined parameters. There are three assumptions about the undetermined parameters K_d and n_d: (1) K_d is a function of Z parameter[9]; (2) both K_d and n_d are the function of Z parameter[20]; (3) K_d and n_d are constants under different deformation conditions[21].

It can be seen from Fig.2 that $\Delta\sigma$ of the curve σ_{DRX} deviating from the curve σ_{DRV} represents the softening degree of DRX, and the maximum value is ($\sigma_{sat} - \sigma_{ss}$). Therefore, the DRX volume fraction can be expressed as follows:

$$X_{DRX} = \frac{\Delta\sigma}{\sigma_{sat} - \sigma_{ss}} = \frac{\sigma_{DRV} - \sigma_{DRX}}{\sigma_{sat} - \sigma_{ss}} \quad (11)$$

where σ_{DRV} is the flow stress when DRV is the main softening mechanism; σ_{DRX} is the flow stress in the DRX stage; σ_{sat} is the saturation stress resulting from the balance between WH and DRV; σ_{ss} is the steady-state stress due to DRX. σ_{DRV} can be calculated by Eq.(9). By combining Eq.(10) with Eq.(11), the expression of flow stress in DRX stage can be obtained, as follows:

$$\sigma_{DRX} = \sigma_{DRV} - \left(\sigma_{sat} - \sigma_{ss}\right) \times \left\{1 - \exp\left[-K_d\left(\frac{\varepsilon - \varepsilon_c}{\varepsilon_p}\right)^{n_d}\right]\right\} \quad (\varepsilon \geq \varepsilon_c) \quad (12)$$

Acoording to Eq.(12), there are five unknown parameters, including ε_c, ε_p, σ_{ss}, K_d, and n_d. Peak strain can be easily obtained from the flow stress curves. Fig. 7 shows the relationship between ε_p and Z parameter, so ε_p can be expressed as a function of Z parameter:

$$\varepsilon_p = 0.0058Z^{0.0970} \quad (13)$$

Fig.8 shows the relationship between critical strain ε_c and Z parameter. Similarly, the critical strain ε_c can be expressed as a function of the Z parameter, as follows:

$$\varepsilon_c = 0.0040Z^{0.0877} \quad (14)$$

Fig. 9 shows the dependence of the steady-state stress σ_{ss} on the peak stress σ_p. Through the linear fitting method, the relationship between σ_{ss} and σ_p can be obtained, as follows:

$$\sigma_{ss} = 0.7346\sigma_p - 12.0531 \quad (15)$$

Substituting the experiment data after the critical strain into Eq.(12), and the relationship between $\ln[(\varepsilon-\varepsilon_c)/\varepsilon_p]$ and $\ln[-\ln(1 - X_{DRX})]$ can be obtained. As shown in Fig. 10, under the condition of 250 °C/0.001 s^{-1}, the parameter n_d can be obtained from the slope of the fitting curve, and the parameter K_d can be obtained from the intercept of the fitting curve. The calculated n_d value ranges from 1.08 to 1.65, and its average value is 1.34. The relationship between K_d and Z parameter is shown in Fig. 11. It is obvious that K_d can be expressed as a function of the Z parameter, as follows:

$$K_d = 0.0040Z^{0.1295} \quad (16)$$

Therefore, the constitutive equations for the AZ80

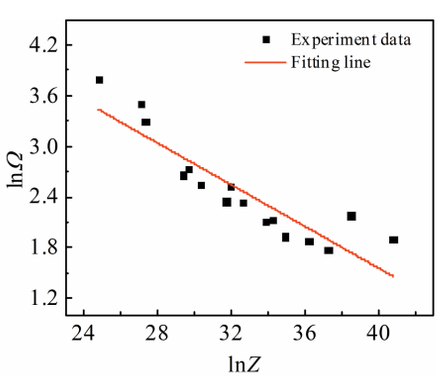

Fig.6 Relationship between lnΩ and ln$Z$

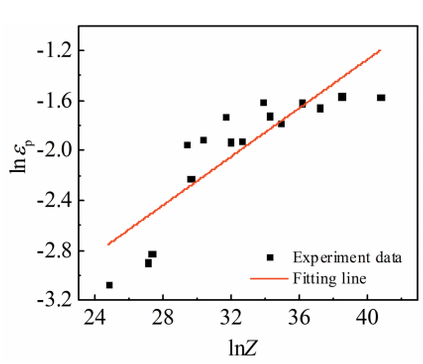

Fig.7 Relationship between lnε_p and ln$Z$

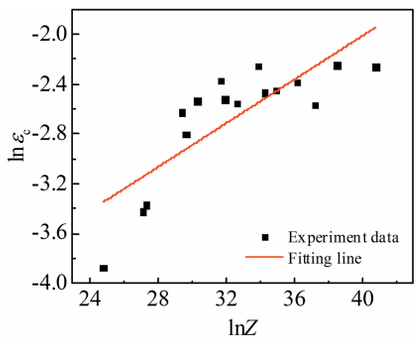

Fig.8 Relationship between lnε_c and ln$Z$

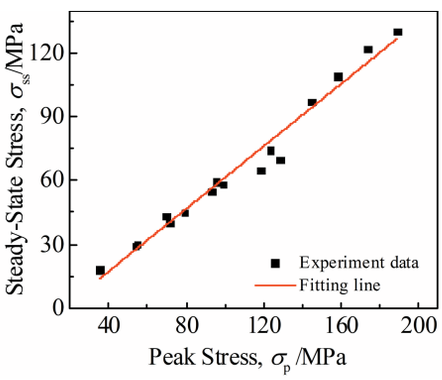

Fig.9 Relationship between steady-state strain σ_{ss} and peak strain σ_p

magnesium alloy during the DRX stage ($\varepsilon \geq \varepsilon_c$) can be expressed by Eq.(17), as follows:

$$\begin{cases} \sigma_{DRX} = \sigma_{DRV} - (\sigma_{sat} - \sigma_{ss})\left\{1 - \exp\left[-k_d\left(\dfrac{\varepsilon - \varepsilon_c}{\varepsilon_p}\right)^{n_d}\right]\right\} \\ \sigma_{DRV} = \left[\sigma^2_{sat} + \left(\sigma^2_0 - \sigma^2_{sat}\right)e^{-\Omega\varepsilon}\right]^{0.5} \\ \sigma_{sat} = -23.8786 + 1.4420\sigma_p \\ \sigma_0 = 0.1465\ln Z - 22.104 \\ \Omega = 68.8851Z^{-0.064\,51} \\ \sigma_{ss} = 0.7346\sigma_p - 12.0531 \\ \varepsilon_p = 0.0058Z^{0.0970} \\ \varepsilon_c = 0.0040Z^{0.0877} \\ K_d = 0.0040Z^{0.1295} \\ n_d = 1.34 \\ Z = \dot{\varepsilon}\exp(177\,332/RT) \end{cases} \quad (17)$$

3.2 Establishment of BP ANN model

Using Matlab neural network platform, the feed-forward BP ANN model based on L-M training algorithm was used to study the flow behavior of AZ80 magnesium alloy. The network model consisted of an input layer, a hidden layer, and an output layer. Among the layers, the input layer has three nodes, which are deformation temperature T, strain rate $\dot{\varepsilon}$, and strain ε; the output layer has one node, which is the flow stress σ.

The operating mechanism of BP neural network model is to calculate the error by comparing the calculated results of feed-forward network with the experiment values, and adjust the mass of each neuron through BP of error for obtaining the desired output. The process to iteratively minimize the mean square error is called network training. The masses of the trained network are stored and can be used to predict the output of a given set of different inputs later.

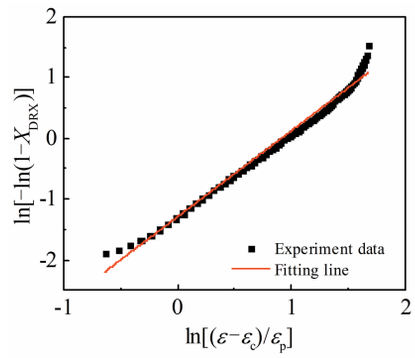

Fig.10 Relationship between ln[−ln(1−X_{DRX})] and ln[(ε−ε_c)/ε_p]

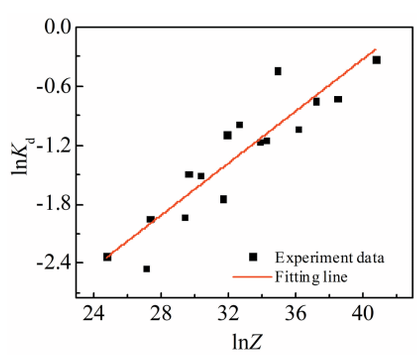

Fig.11 Relationship between lnK_d and ln$Z$

In the ANN model, the selection of hidden layer nodes is usually a complicated problem. If the number of hidden layer nodes is small, the model cannot achieve the effective training or accurately predict the specimens which are not involved in training. If the number of hidden layer nodes is large, it will lead to a longer learning time, even overfitting, and the error may not reach the optimization. Therefore, there should be an optimal number of hidden layer nodes. The formula for selecting the number of hidden layer nodes is expressed by Eq.(18), as follows:

$$k = \sqrt{m + n} + a \quad (18)$$

where k is the number of nodes of the hidden layer, m is the number of neurons in the input layer, n is the number of neurons in the output layer, and a is a constant between 1 and 10. The number of hidden layer neurons is determined by repeated trials and error comparisons. It is found that a network structure with 2 hidden layers of 5 and 3 neuron nodes separately has the best prediction performance. Its structure is 3×5×3×1, as shown in Fig.12.

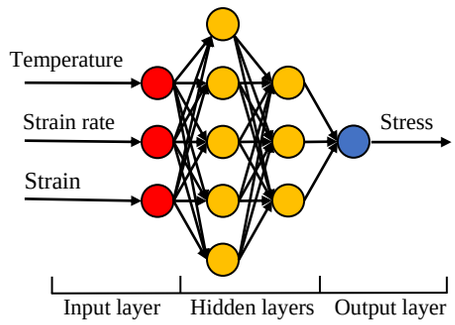

Fig.12 Structure of feed-forward ANN model for AZ80 magnesium alloy

Among 16 groups of true stress-true strain curves, 80% data were randomly selected as training specimens, i.e., 12 groups of true stress-true strain curves were selected. The remaining 4 groups were used as test specimens. The training specimens of 91 were selected for each flow stress curve, and the total number of training specimens was 1092, as shown in Table 2. And from the 16 curves, 288 points were selected from the true strain from 0.05 to 0.9 with strain interval of 0.05 as test data to test the prediction ability of the BP ANN model.

According to the requirements of the network for input and output data, if the data of different sizes act on the input nodes of the network at the same time, the effect of small data on the function is inevitably annihilated, resulting in the difficulties in adjusting the masses between the hidden layer and the input layer, and thereby affecting the convergence speed and accuracy of the network. In order to overcome this shortcoming, the input data should be normalized firstly, so the input value is between −1 and 1. Then the output data should be denormalized. The input and output data are normalized and denormalized according to Eq.(19) and Eq.(20), as follows:

$$X_{\mathrm{n}} = \left(X - X_{\min}\right) / \left(X_{\max} - X_{\min}\right) \tag{19}$$

$$X = X_{\min} + X_{\mathrm{n}}\left(X_{\max} - X_{\min}\right) \tag{20}$$

where X is the original experimental data; $X_{\min}$ and $X_{\max}$ are the minimum and maximum values of specimen data, respectively; X_{n} is the normalized data.

In this research, the training goal of the ANN model was set as 10^{-5}, and the learning rate was 0.03. Since the neural network may not always find the appropriate mass of the optimal solution, re-training of 30 times of the ANN model was conducted to find the solution[22]. After 156 iterations, the system converges and the system error reaches the training goal.

Table 2 Selection status of training specimens and test specimens

Temperature/°C	Strain rate/s^{-1}			
	0.001	0.01	0.1	1
250	Train	Train	Train	Train
300	Train	Test	Train	Test
350	Test	Train	Test	Train
400	Train	Train	Train	Train

4 Prediction Results

The prediction results of the flow stress of two models are shown in Fig. 13. It can be found that both models can well predict the high temperature flow stress of the alloy. However, the prediction accuracy of BP ANN model is obviously better than that of the physical-based constitutive model, according to the fact that the prediction results of ANN model are the closer to the experiment data.

In order to evaluate the prediction accuracy of the two models systematically, three statistical indexes, correlation coefficient (R), AARE, and relative error (RE), were used as the evaluation criteria for the model accuracy in this research. R reflects the linear correlation strength between the experiment value and the predicted value; AARE is an unbiased statistical parameter to verify the predictability of the constitutive model. The expressions of R, AARE, and RE are as follows:

$$\begin{cases} R = \dfrac{\sum_{i=1}^{N}\left(X_i - \bar{X}\right)\left(Y_i - \bar{Y}\right)}{\sqrt{\sum_{i=1}^{N}\left(X_i - \bar{X}\right)^2}\sqrt{\sum_{i=1}^{N}\left(Y_i - \bar{Y}\right)^2}} \\ \mathrm{AARE} = \dfrac{1}{N}\sum_{i=1}^{N}\left|\dfrac{X_i - Y_i}{X_i}\right| \times 100\% \\ \mathrm{RE} = \dfrac{X_i - Y_i}{X_i} \times 100\% \end{cases} \tag{21}$$

where X_{i} and Y_{i} are the experiment stress and the predicted stress, respectively; $\bar{X}$ and $\bar{Y}$ are the averages of X_{i} and Y_{i}, respectively; N is the number of data points used for fitting.

Fig. 14 shows the correlation between the predicted values and the experiment values of two models. R and AARE of the physical-based constitutive model are 0.9936 and 4.52%, respectively; while those of the BP ANN model are 0.9991 and 2.02%, respectively.

As shown in Fig.15, the statistical analysis of RE of the two models shows that the range of RE between the predicted value and the experiment value of the physical-based model is −14%~18%, which is wider than that of the BP ANN model (−5.5%~5.5%). Meanwhile, the number of experiment points of RE range between −4%~4% of the physical-based constitutive model is 181, which is less than that of BP ANN model (279). In summary, the prediction accuracy of the BP ANN model is higher than the physical-based constitutive model. The comparison results of prediction accuracy of the two models are shown in Table 3.

5 Comparison and Discussion of Constitutive Models

The fair prediction ability of the physical-based model is attributed to the clear physical meaning. However, there are many physical parameters in this model which need to be considered, resulting in many independent parameters in the model and the fact that the calculation process is relatively

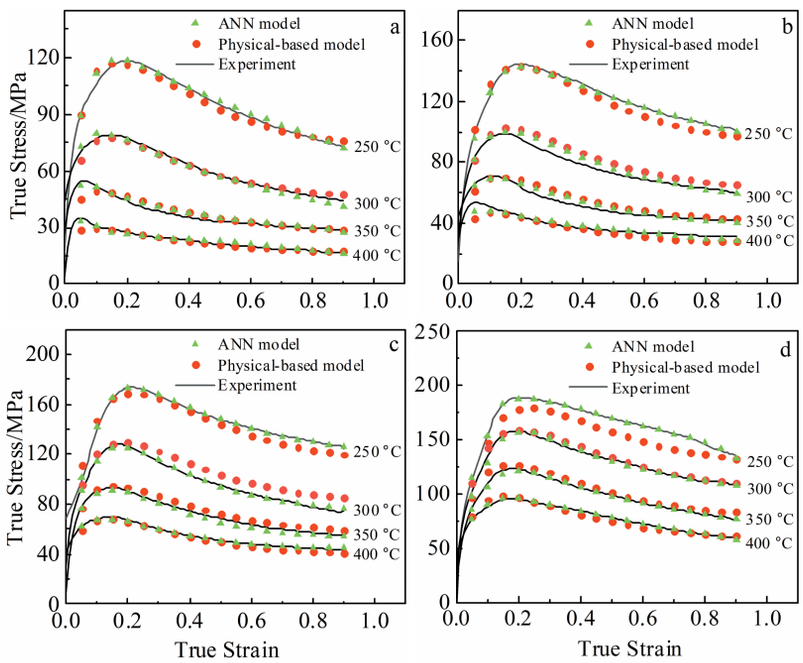

Fig.13 Comparison between experiment results and predicted flow stresses of physical-based constitutive model and ANN model at different strain rates: (a) $\dot{\varepsilon}$=0.001 s^{-1}, (b) $\dot{\varepsilon}$=0.01 s^{-1}, (c) $\dot{\varepsilon}$=0.1 s^{-1}, and (d) $\dot{\varepsilon}$=1 s^{-1}

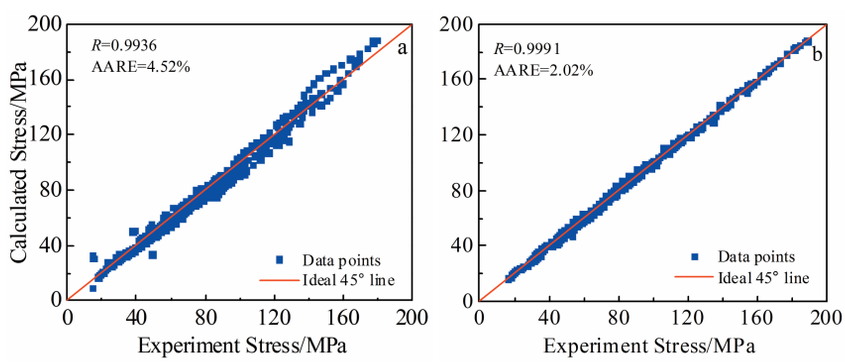

Fig.14 Correlations between predicted values and experiment results of physical-based constitutive model (a) and ANN model (b)

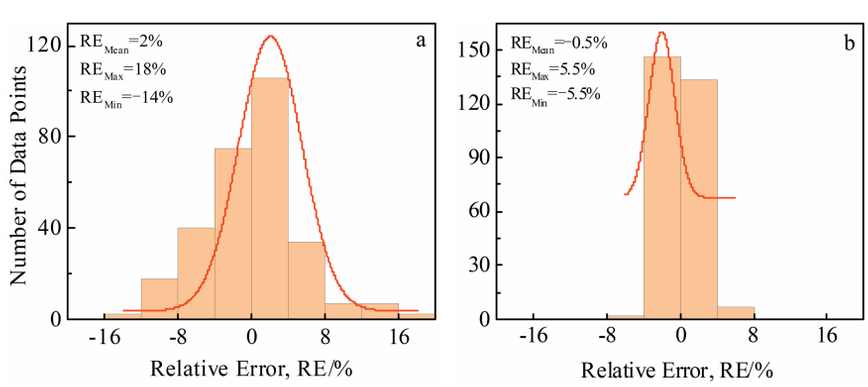

Fig.15 Relative error RE between predicted values and experiment results of physical-based constitutive model (a) and ANN model (b)

Table 3 Comparison of predicted and experiment values by physical-based constitutive model and BP ANN model

Model	*R*	AARE/%	RE/%	Number of data points in RE range of −4%~4%
Physical-based constitutive model	0.9936	4.52	−14~18	181
BP ANN model	0.9991	2.02	−5.5~5.5	279

complicated. In addition, there is a problem of smoothness at the critical strain, i.e., when the values of the parameters K_d and n_d are inappropriate, the flow stress curve tends to have a sharp angle, which reduces the accuracy and practicability of the physical-based constitutive model.

In contrast, the better prediction ability of ANN model is attributed to its ability to deal with complex nonlinear relationships. It can effectively and accurately predict the flow stress of different materials without considering the calculation process of parameters. However, it should also be found that the neural network model cannot provide an accurately defined mathematical formula for subsequent finite element simulation, and the determination of the number of hidden layers and the number of neurons in the model is relatively complicated. Therefore, it is necessary to determine the optimal hidden layer structure through repeated trials and error calculations in order to obtain the desired output.

6 Conclusions

1) The prediction ability of backpropagation (BP) artificial neural network (ANN) model is better than that of physical-based constitutive model.

2) The fair predictive ability of the physical-based constitutive model is attributed to the clear physical meaning. However, many physical parameters need to be considered in the model, and the calculation process is relatively complicated. Particularly, when the values of undetermined parameters K_d and n_d are inappropriate, sharp angles are prone to appear at the critical strain in the model, thus reducing the accuracy and practicability of the model.

3) The better prediction ability of ANN model is attributed to its ability to deal with complex nonlinear relationships. However, this model cannot provide an accurately defined mathematical formula for subsequent finite element simulation, and the determination of the number of hidden layers and the number of neurons in the model is relatively complicated.

References

1 Zhou H T, Li Q B, Zhao Z K *et al. Materials Science and Engineering A*[J], 2010, 527(7-8): 2022

2 Chen Shenghui. *Thesis for Master*[D]. Xi'an: Northwestern Polytechnical University, 2004 (in Chinese)

3 Feng J M, Eliane G, Cao X D *et al. Journal of Plasticity Engineering*[J], 2017, 24(6): 151 (in Chinese)

4 Lin Y C, Chen X M. *Materials & Design*[J], 2011, 32(4): 1733

5 Yu D H. *Materials & Design*[J], 2013, 51: 323

6 Chen G, Chen W, Ma L *et al. Rare Metal Materials and Engineering*[J], 2015, 44(9): 2120

7 Lin Y C, Chen M S, Zhong J. *Mechanics Research Communications*[J], 2008, 35(3): 142

8 Wu B, Li M Q, Ma D W. *Materials Science and Engineering A* [J], 2012, 542: 79

9 Lin Y C, Chen X M, Wen D X *et al. Computational Materials Science*[J], 2014, 83: 282

10 Peng W W, Zeng W D, Wang Q J *et al. Materials & Design*[J], 2013, 51: 95

11 Haghdadi N, Zarei-Hanzaki A, Khalesian A R *et al. Materials & Design*[J], 2013, 49: 386

12 Yan L M, An D, Shi G *et al. Journal of Materials Engineering and Performance*[J], 2017, 26(5): 2368

13 Sun C H, Sun Z H, Zhao J Q *et al*. *Rare Metal Materials and Engineering*[J], 2020, 49(6): 1885

14 Laasraoui A, Jonas J J. *Metallurgical Transactions A*[J], 1991, 22(7): 1545

15 Mecking H, Kocks U. *Acta Metallurgica*[J], 1981, 29(11): 1865

16 Ji G L, Li F G, Li Q H *et al*. *Materials Science and Engineering A*[J], 2010, 527(9): 2350

17 Zener C, Hollomon J H. *Journal of Applied Physics*[J], 1944, 15(1): 22

18 Li Quan, Luo Xiaodong, Jin Zhaoyang. *Journal of Plasticity Engineering*[J], 2020, 27(10): 130 (in Chinese)

19 Ponge D, Gottstein G. *Acta Materialia*[J], 1998, 46(1): 69

20 Jin Zhaoyang, Cui Zhenshan. *Journal of Shanghai Jiaotong University*[J], 2010, 44(4): 437 (in Chinese)

21 Cai Bin, Sun Zhaoyang, Wan Li *et al*. *Acta Metall Sinica*[J], 2016, 52(9): 1123 (in Chinese)

22 Zhao J W, Ding H, Zhao W J *et al. Computational Materials Science*[J], 2014, 92: 47

物理基本构模型和BP人工神经网络模型预测AZ80镁合金高温流动应力的比较研究

李　全，金朝阳

(扬州大学 机械工程学院，江苏 扬州 225127)

摘　要：基于变形温度250~400 ℃和应变速率0.001~1 s^{-1}条件下的铸态AZ80镁合金的热压缩试验数据，建立了基于应力位错关系和动态再结晶动力学的物理基本构模型以及前馈反向传播算法的人工神经网络（ANN）模型来预测AZ80镁合金的热变形行为。采用相关系数（*R*）、平均绝对相对误差（AARE）、相对误差（RE）3种统计学指标来验证2种模型的预测精度。结果表明，2种模型均可以准确预测AZ80镁合金的热变形行为。其中，ANN模型预测的应力值与实验数据更为吻合，其*R*和AARE分别为0.9991和2.02%，而物理基本构模型预测的*R*和AARE分别为0.9936和4.52%。ANN模型较好的预测能力归功于它擅长处理复杂的非线性关系，而物理基本构模型的预测能力是基于模型具有一定的物理意义，模型参数的确定充分考虑了热变形过程中的加工硬化（WH）、动态回复（DRV）和动态再结晶（DRX）的热动力学机制。最后，对这2种本构模型的优缺点及适用范围进行了比较讨论。

关键词：AZ80镁合金；物理基本构模型；人工神经网络模型

作者简介：李　全，男，1993年生，硕士，扬州大学机械工程学院，江苏 扬州 225127，E-mail：quanli1993@qq.com